Journal of Biomechanics 48 (2015) 2090–2095

Contents lists available at ScienceDirect

Journal of Biomechanics

journal homepage: www.elsevier.com/locate/jbiomech
www.JBiomech.com

Numerical analysis of Venous External Scaffolding Technology for Saphenous Vein Grafts

T. Meirson [a,*], E. Orion [b], I. Avrahami [c]

[a] Department of Medical Engineering, Afeka Academic College of Engineering, Tel Aviv, Israel
[b] Vascular Graft Solutions Ltd., Tel Aviv 6971921, Israel
[c] Department of Mechanical Engineering & Mechatronics, Ariel University, Israel

ARTICLE INFO

Article history:
Accepted 10 March 2015

Keywords:
CFD
VEST
CABG
Saphenous vein
Hemodynamics

ABSTRACT

This paper presents a method for analyzing and comparing numerically Saphenous Vein Grafts (SVGs) following Coronary Artery Bypass Graft surgery (CABG). The method analyses the flow dynamics inside vein grafts with and without supporting using Venous External Scaffolding Technology (VEST). The numerical method uses patients' specific computational fluid dynamics (CFD) methods to characterize the relevant hemodynamic parameters of patients' SVGs. The method was used to compare the hemodynamics of six patient's specific model and flow conditions of stented and non-stented SVGs, 12 months post-transplantation. The flow parameters used to characterize the grafts' hemodynamics include Time Averaged Wall Shear Stress (TAWSS), Oscillatory Shear Index (OSI) and Relative Residence Time (RRT). The effect of stenting was clearly demonstrated by the chosen parameters. SVGs under constriction of VEST were associated with similar spatial average of TAWSS (10.73 vs 10.29 dyn/cm^2), yet had fewer lesions with low TAWSS, lower OSI (0.041 vs 0.08) and RRT (0.12 vs 0.24), and more uniform flow with less flow discrepancies. In conclusion, the suggested method and parameters well demonstrated the advantage of VEST support. Stenting vein grafts with VEST improved hemodynamic factors which are correlated to graft failure following CABG procedure.

1. Introduction

Cardiovascular disease remains the leading cause of death in the U.S (Murphy et al., 2013). The treatment of choice for patients with severe coronary artery disease is Coronary Artery Bypass Grafting (CABG) surgery (Mohr et al., 2013). The most commonly used conduits in CABG procedures, the Greater Saphenous Veins (GSVs), suffer from relatively low patency rates. Early vein graft failure occurs in as many as 20% of the cases within the first year post-surgery. Late vein graft failure 5–10 years after surgery, occurs in more than 40% of vein grafts, while only 50% of the patent vein grafts are free of significant stenosis (Motwani and Topol, 1998). The main reason for late vein graft failure is intimal hyperplasia that eventually leads to graft occlusion. Vein graft failure significantly increases the patient's risk for myocardial infarction or death and may result in cardiac re-interventions such as percutaneous coronary interventions and redo CABG operations (Motwani and Topol, 1998).

Vein failure due to intimal hyperplasia is often attributed to graft hemodynamics. Regions with low and oscillatory Wall Shear Stress (WSS), as in the case of lumen irregularities and curvatures, are more susceptible to aggressive intimal hyperplasia foci (Bluestein et al., 1999; Chatzizisis et al., 2007; Davies, 2009; Kassab and Navia, 2006; Malek et al., 1999). On the other hand, physiological level of WSS with uniform directed flow is beneficial in preventing advancement of intimal hyperplasia (Chiu and Chien, 2011).

To characterize the different flow environments acting on the inner wall of the CABG conduit, several hemodynamic parameters have been developed and investigated. These parameters, which include low WSS, high Oscillatory Shear Index (OSI) (Chatzizisis et al., 2011; Ethier, 2002; Ku et al., 1985; Samady et al., 2011) and high Relative Residence Time (RRT) (Himburg et al., 2004; Lee et al., 2009) have been shown to be associated with atherosclerotic disease. The frictional force determined by blood flow impacting on the endothelium is represented by WSS, while OSI represents the oscillation in both magnitude and direction of WSS and RRT indicates the relative time of residence the particle spent at endothelium (Himburg et al., 2004). Disturbed flow with vortices is characterized with changes in flow direction with time and space, including flow separation and reattachment.

To eliminate the fluid dynamic triggers of intimal hyperplasia, the concept of a constrictive external support mesh applied during surgery for vein grafts was suggested as early as in 1963 (Human et al., 2009). Several groups have showed that external support of

* Corresponding author: Tel.: +972 505 666058.
E-mail address: tomermrsn@gmail.com (T. Meirson).

http://dx.doi.org/10.1016/j.jbiomech.2015.03.011
0021-9290/

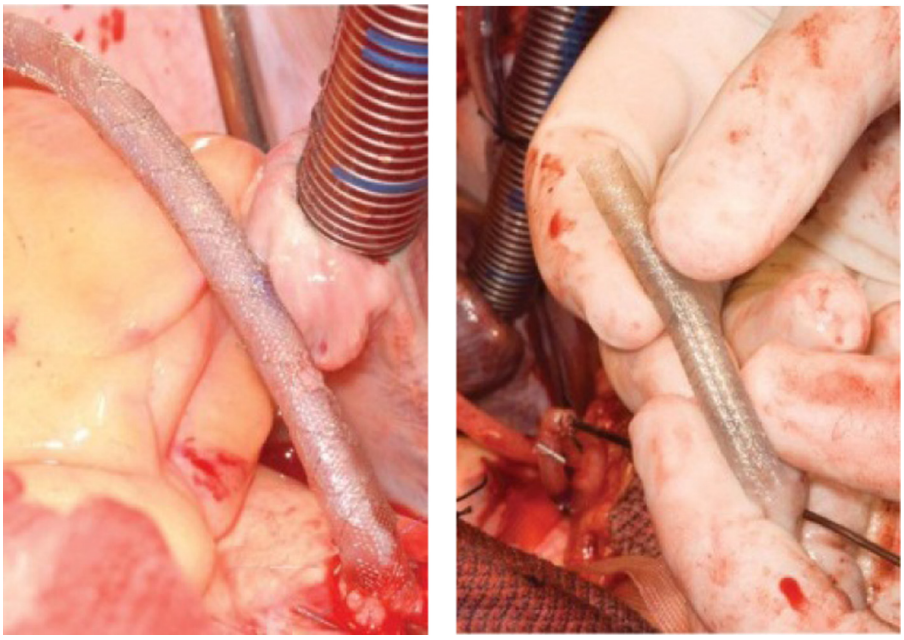

Fig. 1. Stented vein graft with VEST (left) and the VEST device (right) (Vascular Graft Solutions, Tel Aviv, Israel).

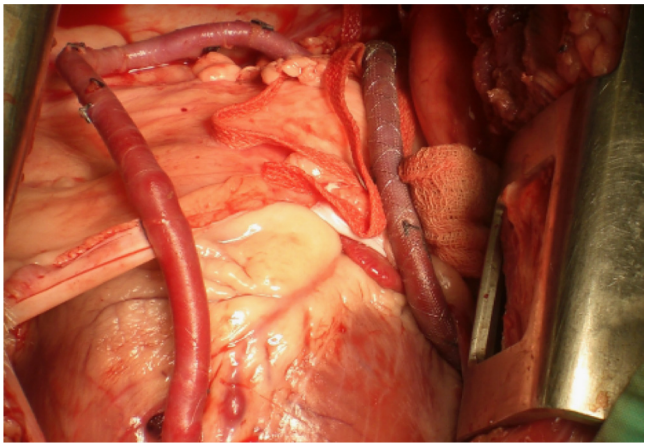

Fig. 2. Image of a stented (left) and non-stented vein graft (right).

SVGs significantly mitigates intimal hyperplasia and medial thickening (Angelini et al., 2002; Krejca et al., 2002; Zurbrugg et al., 1999) by preventing dilatations, reduction of wall tension and prevention of flow disturbances. The Venous External Scaffolding Technology or VEST (Vascular Graft Solutions Ltd., Tel Aviv, Israel) is a cobalt–chromium braided mesh with a unique combination of different wire types (Taggart et al., in press). The VEST can elongate without recoil to cover the entire length of a vein graft and provides mildly constrictive radial support while maintaining crush and kink resistance. The device is applied externally to the vein graft during surgery in less than a minute without affecting the current grafting technique. Examples of VEST deployed over SVGs are shown in Figs. 1 and 2.

Computational fluid dynamics (CFD) is the most common method to explore complex flow mechanics and to investigate the WSS distribution in vessels, including coronary arteries and bypass grafts (Nordgaard et al., 2010). Combining various topographic and anatomic features with real and theoretical hemodynamic conditions using computer based modeling provides a mechanism to investigate these potential interactions (Ricotta et al., 2008). Therefore, the aim of the present study is to introduce and establish a patient-specific CFD method to investigate numerically the hemodynamics of stented and non-stented SVG and to calculate the different corresponding flow parameters. The presented model is the first to analyze and compare hemodynamics of patients' based grafts with external support device using CFD.

Table 1
List of grafts' models.

Graft type	Bypass	Symbol
Control	RCA	A
Control	RCA	B
Control	LCx	C
Support	RCA	D
Support	RCA	E
Support	LCx	F

RCA–Right coronary artery, LCx–Left circumflex

2. Methods

2.1. Model reconstruction

Six numerical models of unsupported (A, B and C) and supported (D, E and F) vein grafts were built based on patients' data. The geometry reconstructions of the models were based on 6 angiographic images, collected from VEST trial (Taggart et al., in press) 12 months post-transplantation, as listed in Table 1. The first step was to reconstruct 3D geometric models from the images. An example of a model geometry reconstruction can be seen in Fig. 3. Reconstruction of the grafts excluded anastomoses and the graft was assumed planar and axisymmetric (Dur et al., 2011; Katritsis et al., 2010; Mohammadi and Bahramian, 2009; Shim et al., 2000), except clear asymmetric luminal irregularities. Grafts dimensions were calibrated using the diameter of the catheter. The geometry reconstruction utilized the commercial software SOLIDWORKS.

2.2. The numerical models

The flow was assumed 3D, time-dependent, incompressible and laminar (Nordgaard et al., 2010). Blood was assumed Newtonian and homogenous with viscosity of 3.5 cP and density of 1.056 g/cm^3 (Nordgaard et al., 2010; Santamarina et al., 1998). Gravitational force assumed to be negligible. The governing equations were the continuity equation:

$$\nabla \cdot u = 0 \quad (1)$$

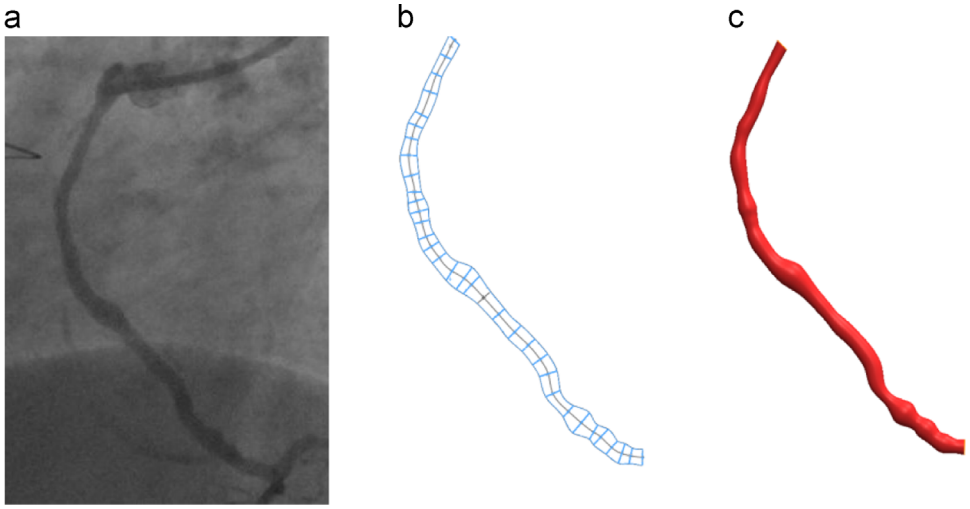

Fig. 3. Graft reconstruction: (a) angiography scan (b) geometry reconstruction and (c) resulted geometric model.

and the Navier–Stokes equation:

$$\rho\frac{\partial u}{\partial t}+\rho(u\cdot\nabla)u=-\nabla p+\mu\nabla^2 u \tag{2}$$

where u is the velocity vector, t is the time, p is the pressure, ρ is the density and μ is the dynamic viscosity.

The boundary conditions for the models included patient's specific flow rate. For each model, the patient's averaged flow rate was used to scale the time-dependent inlet velocity time-function. In order to prevent the effect of heart rate (HR) variations and pulsatility index, all cases used the same velocity waveform (shown in Fig. 4) of typical coronary flow with HR of 60 BPM (Schmidt et al., 2013) and with flat inlet velocity profile (Santamarina et al., 1998). The velocity magnitudes were scaled according to patient's TIMI Grade Flow measurements. The imposed inlet velocity was calculated to be proportional to the graft's inlet cross-section in respect to the average cross section. At the graft outlet, stress free conditions were imposed and the graft walls were assumed rigid with no slip and no penetration conditions.

The commercial software ABAQUS FEA was used to solve the set of fluid equations using the finite-element scheme. The numerical mesh models consisted of about 1 million tetrahedral fluid elements with uniform mesh density. The cardiac cycle was divided into 100 equally spaced time steps of 10 ms. Three cardiac cycles were computed to obtain results independent of the initial conditions. The results of the third calculated cycle were fully periodic. Convergence is achieved when all mass, velocity component and energy changes, from iteration to iteration, achieved less than 10^{-6} error.

2.3. Hemodynamics parameters

The Time-Averaged WSS magnitude (TAWSS) is defined (Lee et al., 2009) as,

$$\mathrm{TAWSS}=\frac{1}{T}\int_0^T |\mathrm{wss}_i|dt \tag{3}$$

where wss_i is the instantaneous shear stress vector, T is the time period of the flow cycle and t is time.

The Oscillatory Shear Index (OSI) clarifies the WSS vector deflection from blood flow predominant direction, during cardiac cycle. Thus, OSI is defined (Ku et al., 1985) as,

$$\mathrm{OSI}=\frac{1}{2}\left\{1-\frac{\left|\int_0^T \mathrm{wss}_i dt\right|}{\int_0^T |\mathrm{wss}_i|dt}\right\} \tag{4}$$

The OSI value can vary from zero, for no-cyclic variation of WSS vector, to 0.5, for 180° deflection of WSS direction.

The Relative Residence Time (RRT) is defined (Himburg et al., 2004) as,

$$\mathrm{RRT}=\frac{1}{\mathrm{TAWSS}\times(1-2\times\mathrm{OSI})} \tag{5}$$

The results are presented as normalized values; therefore the proportionality of RRT is of relative importance. The OSI modifies the TAWSS effects on the RRT at a given region of the inner wall of the conduit. Henceforth, the RRT parameter includes the effects of both OSI and TAWSS. Although RRT highly correlates with TAWSS and OSI, the parameter has more tangible connection to the biological mechanism underlying atherosclerosis (Himburg et al., 2004; Lee et al., 2009).

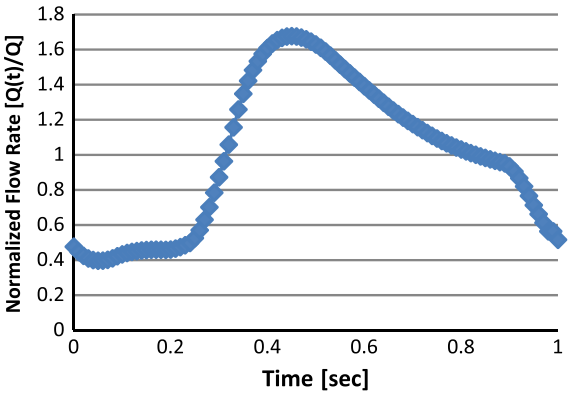

Fig. 4. Normalized coronary inlet pulse wave.

Identification of areas with visible vortices was performed and the number of these areas was noted per graft. Small areas with flow discrepancies were not considered. The observation of vortices was performed on the symmetry plane when the flow is near peak diastole, during time instance 2.5 s.

3. Results

In order to investigate the effect of stented and non-stented grafts on the distribution of hemodynamic parameters, TAWSS, OSI and RRT values were calculated for the grafts wall, and their results during the third cycle ($2\ \mathrm{s} < t < 3\ \mathrm{s}$) are presented in Fig. 5. In addition, Fig. 6 presents examples of regions with disturbed flow of a non-stented graft on the symmetry plane.

Comparison of the TAWSS, as presented at the top row of Fig. 5, demonstrates uniform distribution of stresses in stented grafts compared to the non-stented group. The uniformity is more prominent at grafts D and E. In contrast, non-stented grafts have more variations and fluctuations in stress values. Lower TAWSS are found at dilated or wide areas, while higher values are found at constricted areas. Low values below 4 dyn/cm^2 are pronounced especially at graft C in some areas of graft A and to a lesser extent at graft F, while values above 20 dyn/cm^2 are pronounced at the proximal half of graft B.

Comparisons of the OSI, as presented at the middle row of Fig. 5, demonstrate higher prevalence of values above 0.2 in the non-stented group compared to the stented group. This is prominent especially along grafts A and C. Areas with OSI ranging close to zero, in both

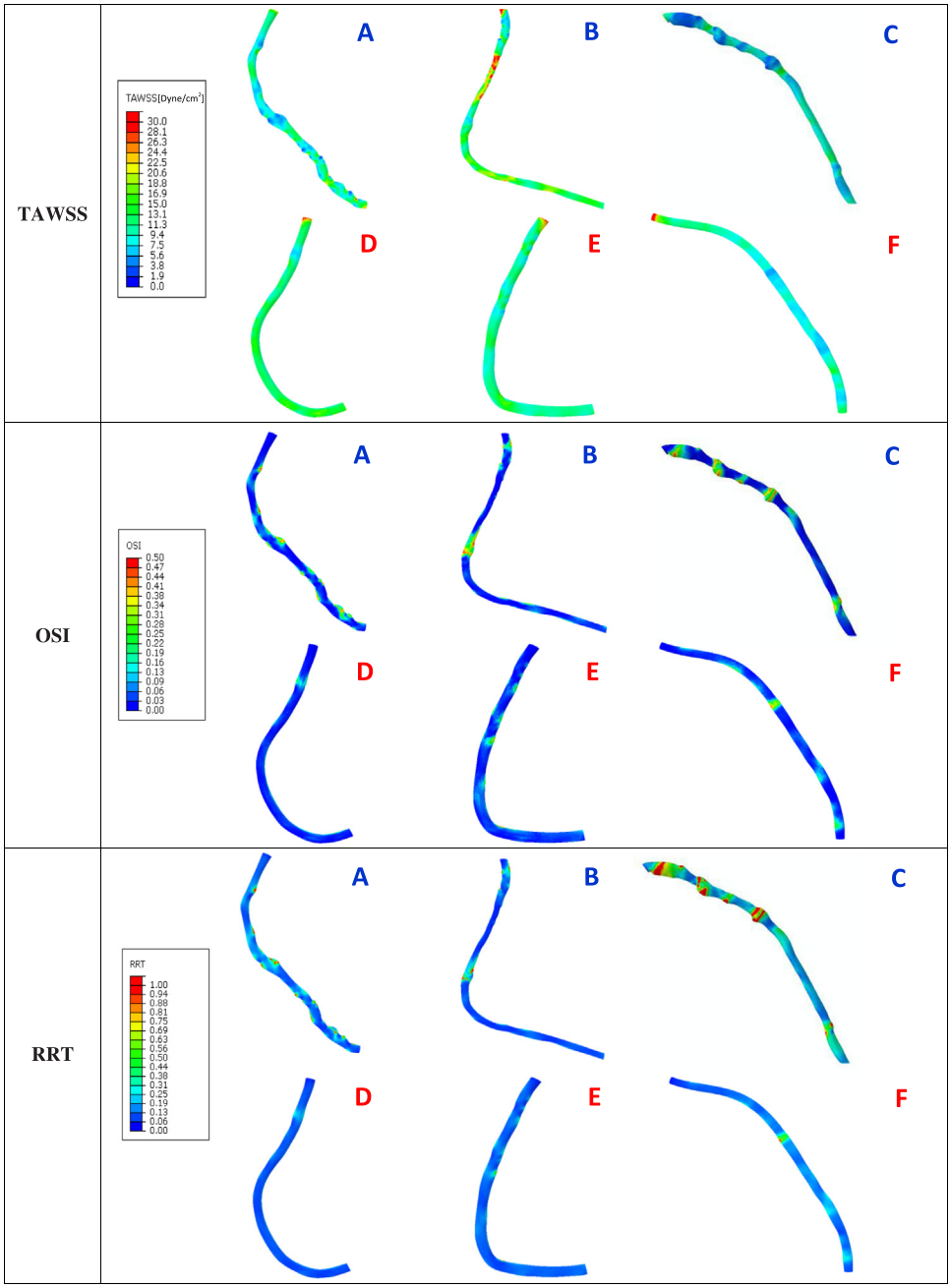

Fig. 5. TAWSS, OSI and RRT results for 6 grafts: control grafts A, B and C (upper row) and supported grafts D, E and F (lower row).

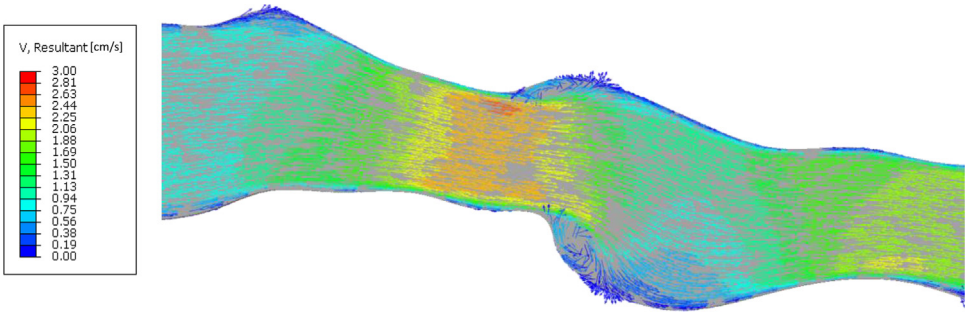

Fig. 6. Visible velocity vortices demonstrating non-uniform flow at two areas of non-stented graft C.

groups, are found along most of the grafts. Highest values close to OSI upper limit of 0.5 are located at the dilated areas at each of the non-stented grafts.

Comparisons of the RRT, as presented at the lower row of Fig. 5, demonstrate similar distribution to OSI results. The stented grafts are characterized with lower RRT values and more uniform

Table 2
Comparison of grafts spatial averages of hemodynamic parameters and No. of vortices.

Type	Symbol	$<$TAWSS$>$ (dyn/cm^2)	$<$OSI$>$	$<$RRT$>$	No. of vortices
Non-stented	A	9.41	0.069	0.203	8
	B	14.23	0.067	0.138	3
	C	7.22	0.094	0.367	5
Average		10.29	0.08	0.24	5.33
Stented	D	12.08	0.030	0.095	0
	E	10.74	0.045	0.114	0
	F	9.36	0.047	0.140	0
Average		10.73	0.041	0.116	0

TAWSS–Time Average Wall Shear Stress. OSI–Oscillatory Shear Index. RRT Relative Residence Time

distributions which range around zero, especially in grafts D and E. The non-stented grafts are characterized with higher RRT values which are mostly found at dilations and luminal irregularities. Maximal RRT values with more extensive distribution are noticeable at graft C with values ranging above 0.8.

Flow disturbances occurred more frequently and more significantly in the non-stented group compared to the stented group. Disturbed flow with recirculation eddies occurred at regions with luminal irregularities. Examples of areas with flow disturbances and vortices can be seen at Fig. 6. The figure shows velocity vectors plot along the non-stented graft C in a cross section view, during near peak flow (t=2.5 s). The plot depicts vortices at two segments where the luminal irregularity occurs. Observation of the vortices shows a clear view of flow separation.

In order to compare the distribution of hemodynamic parameters quantitatively, the spatial average of the grafts' hemodynamic parameters and the number of vortex formations along the graft, are calculated and listed in Table 2. The spatial averages for $<$TAWSS$>$, $<$OSI$>$ and $<$RRT$>$ are calculated by the total integral value of the parameters over the boundary, divided by the number of surface elements, assuming uniform mesh density. The amount of vortices does not distinguish between different vortex sizes.

4. Discussion

The present research includes investigation of the time-dependent flow developed in stented and non-stented SVGs following CABG surgery, using numerical simulations. This study presents patients' specific SVG models based on 3D geometry reconstruction of 2D angiography images 12 months post-transplantation. Boundary conditions of inlet velocity were derived from physical measurements using TIMI frame count collected from the Venous External Support Trial. The use of patient specific anatomical and physiological parameters makes this study as close as possible to real life SVG flow pattern analysis.

The numerical method presented here has a few limitations. The effects of vessel elasticity, fluid–structure interaction and structure–structure interaction between the stent and vessel are not investigated in this study. The wall motion due to cardiac contraction is ignored in this study, as it is shown that the effects of pulsatile flow dominates the TAWSS patterns and hemodynamic aspects, while the motion of the vessel has only minor effect (Zeng et al., 2003). Whereas mean inlet velocity of each model is based on real-life data, inlet pulse wave assumed to follow a typical physiological inlet waveform to eliminate temporal effects of HR and pulsatility. The following factors might also influence the calculations and should be taken into account. Geometrical reconstruction is based on 2D angiographic scans and assumes planar and axisymmetric grafts; blood rheologic properties were simplified; and possible error due to the numerical model. Yet, despite these limitations, the method provides a significant insight on stresses and flow patterns developed in SVGs, and enables the comparison between stented and non-stented vein grafts.

The hemodynamic parameters including TAWSS, OSI and RRT are calculated and vortices are enumerated within 3 stented models and compared with 3 non-stented models. The calculated TAWSS values in the stented grafts were found to be more uniformly distributed with fewer and smaller lesions of low shear stresses as shown in Fig. 5. However, there is no clear trend between the two groups in mean spatial TAWSS as noted in Table 2. This could be expected, as WSS is dominated mainly by the flow rate and the mean diameter of the vessel (Box et al., 2005). The flow depends mostly on the degree of competitive flow and stenosis of the distal anastomosis (Nordgaard et al., 2009, 2010). This result is evidence that the improvement in WSS parameters is not a result of graft narrowing, but a result of improvement in graft geometry. These improvements are best shown by OSI levels. The distributions of both OSI and RRT values were found to be notably lower in the stented grafts (Fig. 5). Similarly, the mean spatial averages of OSI and RRT values for the stented grafts were found to be lower compared to the non-stented group (Table 2). These findings indicate a greater degree of unidirectional flow with less shear stress oscillation along the conduit wall. Correspondingly, the stented group did not develop any visible vortex along the grafts, while the non-stented group has over 5 vortices with complex flow in average. The absence of focal flow disturbances in the stented group strengthens the unidirectional flow pattern while the high prevalence of focal flow disturbances reinforces the multidirectional flow pattern of the non-stented group.

The resulted TAWSS, OSI, RRT and vortex count delineate the effect of local luminal irregularities on the graft's hemodynamics. Examining the hemodynamics reveals the potential mode of action of external support on the flow regime in SVGs. By constricting the vein graft, these meshes provide mechanical support that significantly improves its lumen uniformity (Ben-Gal et al., 2013) through the elimination of luminal irregularities reducing the degree of multidirectional and disturbed flow, and thus may slow progression of venous disease (Chiu and Chien, 2011). This protective effect may slow the progression of venous disease while the unsupported vein grafts may be at higher risk of developing future disease.

5. Conclusions

In order to improve patency rates and decrease Saphenous Vein Graft failure following CABG surgery, the leading causes of intimal hyperplasia should be treated. The numerical method presented may help to understand and establish the advantages of the external mesh support and to evaluate the effects of the external support on the leading causes of graft failure.

Future work

A large scale numerical analysis may provide a wider perspective and statistical significance to the study. Therefore, future work will implement the presented method on all applicable SVGs from VEST trial.

Funding sources

The Venous External Support Trial was funded by Vascular Graft Solutions Ltd. (Tel Aviv, Israel).

Disclosures

Eyal Orion-Co-inventor of VEST, CEO and board member of Vascular Graft Solutions, stock ownership.

Conflict of interest

None.

Acknowledgments

We would like to thank Afeka Academic College of Engineering, Tel Aviv, for their financial support and contribution. We thank Gil Bolotin, Department of Cardiac Surgery, Rambam Health Care Campus, for his assistance.

References

Angelini, G.D., Lloyd, C., Bush, R., Johnson, J., Newby, A.C., 2002. An external, oversized, porous polyester stent reduces vein graft neointima formation, cholesterol concentration, and vascular cell adhesion molecule 1 expression in cholesterol-fed pigs. J. Thorac. Cardiovasc. Surg. 124, 950–956.

Ben-Gal, Y., Taggart, D.P., Williams, M.R., Orion, E., Uretzky, G., Shofti, R., Banai, S., Yosef, L., Bolotin, G., 2013. Expandable external support device to improve Saphenous Vein Graft Patency after CABG. J. Cardiothorac. Surg. 8, 122.

Bluestein, D., Gutierrez, C., Londono, M., Schoephoerster, R.T., 1999. Vortex shedding in steady flow through a model of an arterial stenosis and its relevance to mural platelet deposition. Ann. Biomed. Eng. 27, 763–773.

Box, F.M., van der Geest, R.J., Rutten, M.C., Reiber, J.H., 2005. The influence of flow, vessel diameter, and non-newtonian blood viscosity on the wall shear stress in a carotid bifurcation model for unsteady flow. Investig. Radiol. 40, 277–294.

Chatzizisis, Y.S., Baker, A.B., Sukhova, G.K., Koskinas, K.C., Papafaklis, M.I., Beigel, R., Jonas, M., Coskun, A.U., Stone, B.V., Maynard, C., Shi, G.P., Libby, P., Feldman, C.L., Edelman, E.R., Stone, P.H., 2011. Augmented expression and activity of extracellular matrix-degrading enzymes in regions of low endothelial shear stress colocalize with coronary atheromata with thin fibrous caps in pigs. Circulation 123, 621–630.

Chatzizisis, Y.S., Coskun, A.U., Jonas, M., Edelman, E.R., Feldman, C.L., Stone, P.H., 2007. Role of endothelial shear stress in the natural history of coronary atherosclerosis and vascular remodeling: molecular, cellular, and vascular behavior. J. Am. Coll. Cardiol. 49, 2379–2393.

Chiu, J.J., Chien, S., 2011. Effects of disturbed flow on vascular endothelium: pathophysiological basis and clinical perspectives. Physiol. Rev. 91, 327–387.

Davies, P.F., 2009. Hemodynamic shear stress and the endothelium in cardiovascular pathophysiology. Nat. Clin. Pract. Cardiovasc. Med. 6, 16–26.

Dur, O., Coskun, S.T., Coskun, K.O., Frakes, D., Kara, L.B., Pekkan, K., 2011. Computer-aided patient-specific coronary artery graft design improvements using CFD coupled shape optimizer. Cardiovasc. Eng. Technol. 2, 35–47.

Ethier, C.R., 2002. Computational modeling of mass transfer and links to atherosclerosis. Ann. Biomed. Eng. 30, 461–471.

Himburg, H.A., Grzybowski, D.M., Hazel, A.L., LaMack, J.A., Li, X.M., Friedman, M.H., 2004. Spatial comparison between wall shear stress measures and porcine arterial endothelial permeability. Am. J. Physiol. Heart Circ. Physiol. 286, H1916–H1922.

Human, P., Franz, T., Scherman, J., Moodley, L., Zilla, P., 2009. Dimensional analysis of human saphenous vein grafts: implications for external mesh support. J. Thorac. Cardiovasc. Surg. 137, 1101–1108.

Kassab, G.S., Navia, J.A., 2006. Biomechanical considerations in the design of graft: the homeostasis hypothesis. Annu. Rev. Biomed. Eng. 8, 499–535.

Katritsis, D.G., Theodorakakos, A., Pantos, I., Andriotis, A., Efstathopoulos, E.P., Siontis, G., Karcanias, N., Redwood, S., Gavaises, M., 2010. Vortex formation and recirculation zones in left anterior descending artery stenoses: computational fluid dynamics analysis. Phys. Med. Biol. 55, 1395.

Krejca, M., Skarysz, J., Szmagala, P., Plewka, D., Nowaczyk, G., Plewka, A., Bochenek, A., 2002. A new outside stent—does it prevent vein graft intimal proliferation? Eur. J. Cardiothorac. Surg. 22, 898–903.

Ku, D.N., Giddens, D.P., Zarins, C.K., Glagov, S., 1985. Pulsatile flow and atherosclerosis in the human carotid bifurcation – positive correlation between plaque location and low and oscillating shear-stress. Arteriosclerosis 5, 293–302.

Lee, S.W., Antiga, L., Steinman, D.A., 2009. Correlations among indicators of disturbed flow at the normal carotid bifurcation. ASME. J. Biomech. Eng. 131 (6).

Malek, A.M., Alper, S.L., Izumo, S., 1999. Hemodynamic shear stress and its role in atherosclerosis. JAMA 282, 2035–2042.

Mohammadi, H., Bahramian, F., 2009. Boundary conditions in simulation of stenosed coronary arteries. Cardiovasc. Eng. 9, 83–91.

Mohr, F.W., Morice, M.C., Kappetein, A.P., Feldman, T.E., Stahle, E., Colombo, A., Mack, M.J., Holmes Jr., D.R., Morel, M.A., Van Dyck, N., Houle, V.M., Dawkins, K.D., Serruys, P.W., 2013. Coronary artery bypass graft surgery versus percutaneous coronary intervention in patients with three-vessel disease and left main coronary disease: 5-year follow-up of the randomised, clinical SYNTAX trial. Lancet 381, 629–638.

Motwani, J.G., Topol, E.J., 1998. Aortocoronary saphenous vein graft disease: pathogenesis, predisposition, and prevention. Circulation 97, 916–931.

Murphy, S.L., Xu, J., Kochanek, K.D., 2013. Deaths: final data for 2010. Natl. Vital Stat. Rep. 61, 1–117.

Nordgaard, H., Nordhaug, D., Kirkeby-Garstad, I., Lovstakken, L., Vitale, N., Haaverstad, R., 2009. Different graft flow patterns due to competitive flow or stenosis in the coronary anastomosis assessed by transit-time flowmetry in a porcine model. Eur. J. Cardiothorac. Surg. 36, 137–142, discussion 142.

Nordgaard, H., Swillens, A., Nordhaug, D., Kirkeby-Garstad, I., Van Loo, D., Vitale, N., Segers, P., Haaverstad, R., Lovstakken, L., 2010. Impact of competitive flow on wall shear stress in coronary surgery: computational fluid dynamics of a LIMA-LAD model. Cardiovasc. Res. 88, 512–519.

Ricotta, J.J., Pagan, J., Xenos, M., Alemu, Y., Einav, S., Bluestein, D., 2008. Cardiovascular disease management: the need for better diagnostics. Med. Biol. Eng. Comput. 46, 1059–1068.

Samady, H., Eshtehardi, P., McDaniel, M.C., Suo, J., Dhawan, S.S., Maynard, C., Timmins, L.H., Quyyumi, A.A., Giddens, D.P., 2011. Coronary artery wall shear stress is associated with progression and transformation of atherosclerotic plaque and arterial remodeling in patients with coronary artery disease. Circulation 124, 779–788.

Santamarina, A., Weydahl, E., Siegel Jr., J.M., Moore Jr., J.E., 1998. Computational analysis of flow in a curved tube model of the coronary arteries: effects of time-varying curvature. Ann. Biomed. Eng. 26, 944–954.

Schmidt, R., Graafen, D., Weber, S., Schreiber, L.M., 2013. Computational fluid dynamics simulations of contrast agent bolus dispersion in a coronary bifurcation: impact on MRI-based quantification of myocardial perfusion. Comput. Math. Methods Med. 2013, 13.

Shim, E.B., Kamm, R.D., Heldt, T., Mark, R.G., 2000. Year numerical analysis of blood flow through a stenosed artery using a coupled multiscale simulation method. Comput. Cardiol. 27, 219–222.

Taggart, D.P., Ben Gal, Y., Lees, B., Patel, N., Webb, C., Rehman, S.M., Desouza, A., Yadav, R., De Robertis, F., Dalby, M., Banning, A., Channon, K.M., Di Mario, C., Orion, E. A randomized trial of external stenting for saphenous vein grafts in coronary artery bypass grafting. Ann Thorac Surg. http://dx.doi.org/10.1016/j.athoracsur.2015.01.060, in press.

Zeng, D., Ding, Z., Friedman, M.H., Ethier, C.R., 2003. Effects of cardiac motion on right coronary artery hemodynamics. Ann. Biomed. Eng. 31, 420–429.

Zurbrugg, H.R., Wied, M., Angelini, G.D., Hetzer, R., 1999. Reduction of intimal and medial thickening in sheathed vein grafts. Ann. Thorac. Surg. 68, 79–83.